Journal of Magnetism and Magnetic Materials 527 (2021) 167730

Contents lists available at ScienceDirect

Journal of Magnetism and Magnetic Materials

journal homepage: www.elsevier.com/locate/jmmm

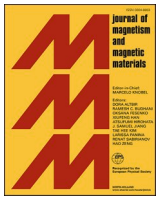

Research articles

Square plate shaped magnetite nanocrystals

S.V. Komogortsev [a,b], S.V. Stolyar [a,c], L.A. Chekanova [b], R.N. Yaroslavtsev [a,*], O.A. Bayukov [b], D. A. Velikanov [b], M.N. Volochaev [b], P.E. Eroshenko [b], R.S. Iskhakov [b]

[a] Krasnoyarsk Scientific Center, Federal Research Center KSC SB RAS, Krasnoyarsk, Russia
[b] Kirensky Institute of Physics, Federal Research Center KSC SB RAS, Krasnoyarsk, Russia
[c] Siberian Federal University, Krasnoyarsk, Russia

ARTICLE INFO

Keywords:
Magnetite
Nanoparticles
Magnetic anisotropy

ABSTRACT

Square plate shaped magnetite nanocrystals have been synthesized by chemical precipitation from solution using arabinogalactan. A high crystal quality was observed in the plate plane while, across the plate, there is some stratification. The magnetic hysteresis in such particles is determined by the bulk magnetocrystalline anisotropy, plate shape anisotropy, and surface magnetic anisotropy. It is shown using the micromagnetic simulation that the ferromagnetic square nanoplates exhibit the extraordinary magnetization switching anisotropy, which should be taken into account for understanding the hysteretic properties of the particles.

1. Introduction

The experience in using magnetite nanoparticles as functional magnetic elements in biomedicine, electronics, catalysis, etc. has shown the importance of a particle shape and structural quality. In the particles with a shape strongly different from spherical, the magnetic moment direction can be stabilized at a smaller particle volume than in the case of a spherical particle. This is due to the contribution of the shape magnetic anisotropy to the total magnetic anisotropy of a particle. In addition, the magnetic properties of particles are affected by their structural quality. For instance, in particles with the easy magnetization axis nonuniform over their volume (amorphous or nanocrystalline particles), the average bulk anisotropy is fairly low [1–3]. Another example is the frustration of exchange interactions between iron atoms at the particle surface, which leads to the formation of a spin glass shell significantly reducing the effective magnetization of a particle [4,5]. The magnetite nanocrystal is a nanoparticle that is structurally ordered inside and has a shape inheriting the symmetry of the crystal lattice. In free magnetite nanocrystals, the (1 1 1) face has the lowest energy, which suggests the formation of triangular or hexagonal crystal faces. However, for a particle in a solution, the energy of the (0 0 1) face in a certain situation may prove to be lower. The evidence from practice shows that the main parameters for controlling the shape are the ligand type and temperature conditions of the synthesis [6]. Meanwhile, the mechanism oblate and prolate nanoparticle synthesis is poorly understood. At present, the synthesis of cubic magnetite nanocrystals is well-proven and the properties of such nanocrystals are well-studied [7–10]. However, since the magnetic anisotropy of the cubic shape is low [11], the magnetic stability of cubic particles differs only slightly from the stability of spherical particles. The oblate and prolate magnetite crystal particles are also synthesized [6,12–14], but, in this case, there is a set of unresolved questions. In particular, the plate-shaped particles are included in a powder containing particles of another different shapes [15–18]. The complexity of obtaining magnetite particles of the uniform shape does not allow one to thoroughly investigate their magnetism. In this work, we report on the synthesis and study of the structure and magnetic properties of magnetite nanocrystals with the shape of square plate.

2. Experimental

All chemicals used in this work had a purity of at least 99%. Magnetite nanoparticles were prepared by chemical precipitation as follows: 5 g of iron sulfate ($FeSO_4 \cdot 7H_2O$), 4 g of disodium salt of ethylenediaminetetraacetic acid (EDTA-Na2), and 0.7 g of arabinogalactan acting as a structural guiding and stabilizing agent were dissolved in 100 ml of distilled water. At a temperature of 80 °C and continuous stirring, NaOH (0.1 M) was added to the solution until a neutral pH was reached, and the color of the solution changed from orange to black. The required temperature was maintained using a water thermostat. Magnetite nanoparticles were washed with distilled water to remove ions and then dried at room temperature.

Electron-microscopic studies were carried out using a Hitachi

* Corresponding author.
E-mail address: yar-man@bk.ru (R.N. Yaroslavtsev).

https://doi.org/10.1016/j.jmmm.2021.167730
Received 13 June 2020; Received in revised form 30 December 2020; Accepted 3 January 2021
Available online 21 January 2021
0304-8853/© 2021 Elsevier B.V. All rights reserved.

HT7700 transmission electron microscope (accelerating voltage 100 kV) of the Center for Collective Use of the Krasnoyarsk Scientific Center. The Mössbauer spectra were measured on an MS-1104Em spectrometer with a source of 57Co (Cr) at room temperature on powder samples with a thickness of 5–10 mg/cm^2 on the basis of the natural iron content. Isomer chemical shifts are accounted in reference to α-Fe. The static magnetic measurements were performed on an automated vibrating sample magnetometer in fields of up to 8 kOe at temperatures from 77 to 300 K. An empty capsule for the sample was measured separately and, then, its contribution (~1%) to the total signal was subtracted.

3. Results and discussion

3.1. Electron microscopy

The transmission electron microscopy images presented in Fig. 1a-1c show that the synthesized nanoparticles are square plate-shaped nanocrystals. The high-resolution images of the surface of individual plates show a system of crystal planes uniformly filling this surface (insert in Fig. 1d).

The distribution of the sides of square nanocrystals (67 particles were counted) fits well with the lognormal function: $f(d) = \frac{1}{d \cdot \sigma\sqrt{2\pi}} \cdot \exp\left(- \ln^2\left(\frac{d}{d_0}\right) \Big/ 2\sigma^2 \right)$ with parameters $d_0 = 64$ nm, $\sigma = 0.48$. Note that d_0, and σ are parameters of the number-weighted distribution. The number-weighted average size is $\langle d \rangle_N = 65 \pm 4$ nm and volume –weighted is $\langle d \rangle_V = 86 \pm 12$ nm. Since $\langle d \rangle_V$ is important for the interpretation of magnetometric data, this size will be used for further estimations and references. The standard error of the mean 12 nm does not characterize the particles well (for example, it depends on the number of particles used for analysis). The 1/2FWHM (full width at half maximum) of the size distribution is 30 nm. The final estimate of the confidence interval for the size of nanoplates is $d = 90 \pm 30$ nm. The thickness of the plates (42 particles were counted) is 10 ± 2 nm.

The cross-sectional images of the plates apparently indicate a cross stratification-type structural defect. A system of diffraction rings in the electron diffraction pattern (Fig. 1e) is consistent with the magnetite reflections. This pattern shows also the reflection corresponding to maghemite. The magnetite nanoparticles in the form of square crystal plates are rarely met. The particles obtained from the vapor phase and some solutions usually have a spherical shape. As was mentioned in Introduction, in free magnetite particles, the formation of triangular or hexagonal crystal faces is energetically more favorable. However, for a particle in a solution, the energy of the (0 0 1) face can appear lower. Obviously, this occurs during the formation of cubic magnetite nanocrystals often used to prepare self-ordered colloids. In our case, the condition of the minimum (0 0 1) face energy and the condition leading to the stratification of a crystal in the system of (0 0 1) planes are apparently combined.

3.2. Mössbauer spectroscopy

The spectrum is well-approximated by four Zeeman sextets (Fig. 2). The spectrum components are shown by color lines. Below this spectrum, the error spectrum, i.e., the difference between the calculated and experimental spectra, is shown. The results of decoding are given in Table 1, where A and B are the tetrahedral and octahedral ferrite sites. The octahedral site linewidths are significantly broadened, which may be indicative of the nonuniform distribution of different-valence cations over these sites. The positions designated as Fe^{3+}(6) can be attributed to the surface sites with a strong fluctuation of the local environment.

The presence of mixed-valence iron $Fe^{2.5+}$ (IS = 0.56 mm/s) shows that we are dealing with magnetite. Under the assumptions of the absence of substitution of other cations for iron and the high quality of the anion lattice, the Mössbauer data allow us to write the spinel formula under the conditions of its electroneutrality as

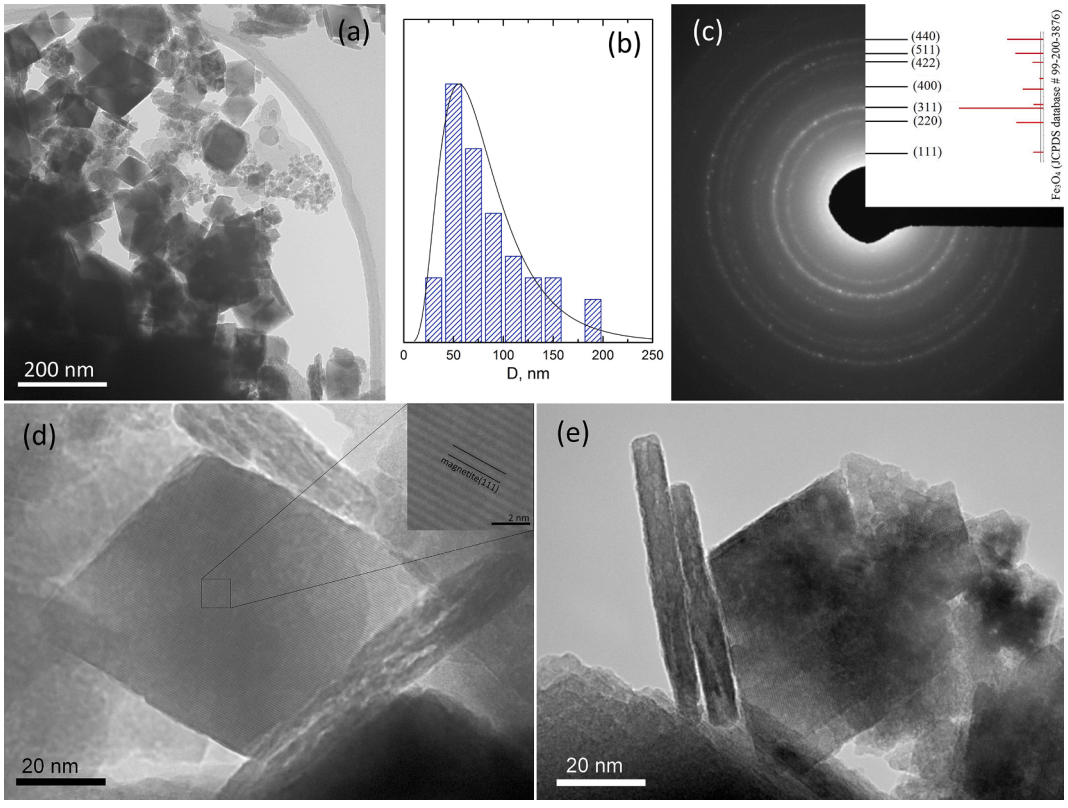

Fig. 1. (a, d, e) TEM images of particles, (b) distributions over square side, (c) and electron diffraction pattern.

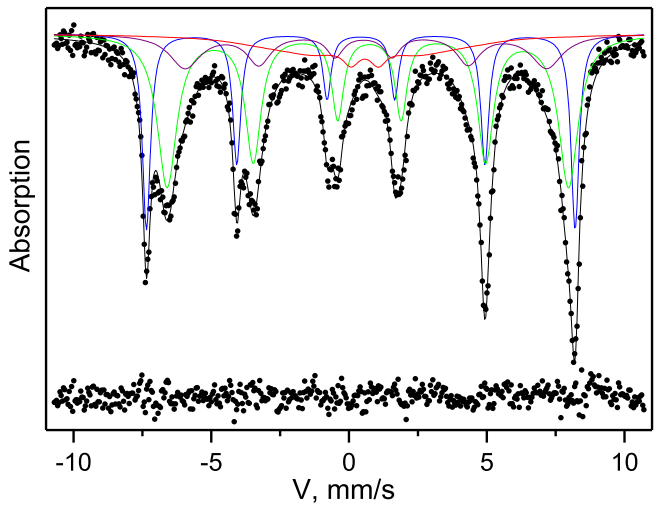

Fig. 2. Mössbauer spectrum of nanoparticles.

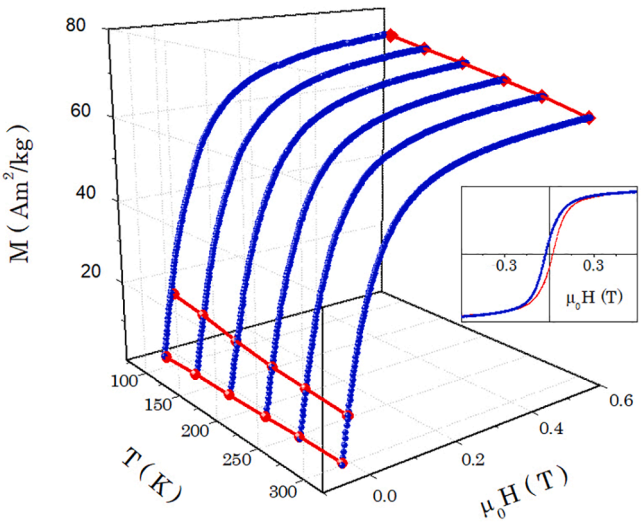

Fig. 3. Magnetization curves for magnetite nanocrystals.

Table 1
Mössbauer parameters. IS is the isomer chemical shift relative to α-Fe, *H* is the hyperfine field on the iron nucleus, QS is the quadrupole splitting, *W* is the absorption linewidth for the internal 34 and external 16 sextet lines, *P* is the fractional population of the site (square under the partial spectrum), and A and B are the tetrahedral and octahedral spinel sites.

IS, mm/ s± 0.01	H, kOe ±5	QS, mm/s ±0.02	$W_{34/16}$, mm/ s ± 0.02	P, fract.% ± 0.03	Site
0.28	483	−0.01	0.36/0.36	0.24	Fe^{3+}(A) magnetite
0.56	452	−012	0.52/0.85	0.46	$Fe^{2.5+}$(B) magnetite
0.42	407	0.17	0.71/1.37	0.16	Fe^{3+}(B) magnetite
0.39	195	−0.11	0.74/4.16	0.14	Fe^{3+}(6)

$$\left(Fe^{3+}\right)\left[Fe^{2+}_{0.658}Fe^{3+}_{1.228}\square_{0.114}O_4\right]$$

where □ is the cationic vacancy. In this approximation, we are dealing with cation-deficient magnetite. Such a system can, in principle, be called a solid solution of magnetite Fe_3O_4 and maghemite γ-Fe_2O_3.

3.3. Magnetic properties

The magnetization curves measured in the applied field range of [−0.6 T, +0.6 T] are symmetric relative to the origin of coordinates and contain a reversible part and an irreversible part, i.e., the hysteresis loop (Fig. 3). The cross sections of the three-dimensional diagram in Fig. 3 show that the coercivity $H_c(T)$, remanent magnetization $M_r(T)$, and magnetization in a field of 0.6 T decrease with increasing temperature.

The quantitative analysis of the reduction of the magnetic hysteresis parameters with increasing temperature is illustrated in Fig. 4.

It is well-known that the coercivity of nanoparticles decreases with increasing temperature and completely vanishes at the blocking temperature T_B, according with Eq. (1) [19]. The best fit of the experimental data by Eq. (1) (the solid line in Fig. 4) yields the following parameters of this equation: $\mu_0 H_c(0) = (32 \pm 2)$ mT, $T_B = (550 \pm 10)$ K, and $\alpha = 0.80 \pm 0.12$.

$$H_c = H_c(0)\cdot(1 - (T/T_B)^{\alpha}) \quad (1)$$

Dependence (1) is characteristic of single-domain noninteracting nanoparticles at temperatures below the blocking temperature T_B [20–22]. The well-known Neel result $H_c \sim T^{1/2}$ corresponds to the parallel orientation of the easy magnetization axes of particles relative to the external magnetic field [23]. Empirical formula (1) is proposed for

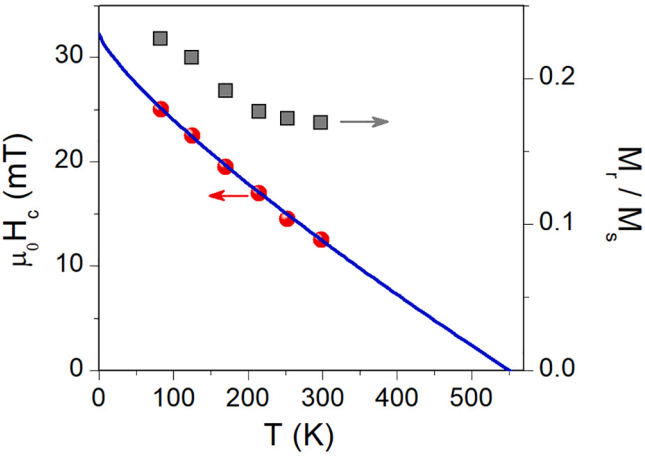

Fig. 4. Coercivity and remanent magnetization in magnetite nanocrystals.

particles with random orientations of the easy magnetization axes. Several teams, using the numerical simulation, estimated the exponent α to be from 0.67 to 1 [19,24–27]. The resulting α estimate for our particles hits this range. The estimated temperature T_B is no higher than the Curie temperature of Fe_3O_4 (840 K); therefore, the description of $H_c(T)$ using Eq. (1) obtained within the thermal relaxation theory is justified here. The remanent magnetization at temperatures from 80 to 300 K decreases by 30%, i.e., much more slowly than H_c (by 100%). Since the anisotropy constant should include contributions from the cubic (magnetocrystalline anisotropy of magnetite) and uniaxial (shape anisotropy), for an ensemble of randomly oriented single-domain particles one would expect remanence (M_r/M_s) values from 0.5 to 0.86 [28]. The fact that the observed value M_r/M_s is less than 0.5 (Fig. 4) can be result from both the dipole–dipole interaction in the system of particles (in Fig. 1 one can see conglomerates of joined particles) and from inhomogeneous states of magnetization in the particle (see Fig. 7).

The portion of the magnetization curve corresponding to approaching the saturation magnetization is often described by the formula

$$M(H) = M_s\cdot\left(1 - a/H - b/H^2\right) + \chi\cdot H \quad (2)$$

Here, the term a/H can be related to the competition of the thermal fluctuations with the external field and the second term b/H^2, to the orientational nonuniformity of the easy magnetization axes in an ensemble of particles. It was found, however, that the strong-field

portions are described much better by Eq. (3) (see Fig. 5) proposed for describing the magnetization curves of iron oxide nanoparticles in [29] and successfully used in [30,31].

$$M(H) = M_s \cdot \left(1 - \frac{H_a^2}{15H^{1/2}\left(H^{3/2} + H_R^{3/2}\right)}\right) + \chi \cdot H \quad (3)$$

The parameters M_s and H_a characterize the magnetization and local anisotropy field of nanoparticles. The change in the M_s value with temperature is described by the Bloch's law $T^{3/2}$ (Fig. 6):

$$M_s(T) = M_{s0} \cdot \left(1 - B \cdot T^{3/2}\right) \quad (4)$$

Here, the fact of observing the Bloch's law $T^{3/2}$ is curious. The point is that, for magnetic particles in general and for magnetite nanoparticles in particular, the deviations from the Bloch's law are theoretically predicted and observed. The change in the magnetization with temperature is still described by the power law $M \propto T^{\alpha}$, but with the exponent α significantly different from 3/2. These deviations are attributed to both the effect of the thermal fluctuations ($\alpha < 3/2$) [32–34] and the effect of confinement in nanoparticles ($\alpha > 3/2$) on the spin-wave excitation spectrum [35,36]. To fit the data in Fig. 5, we chose Eq. (4) for two reasons. First, in our case, the exponent α was very close to 3/2 (the fitting with an arbitrary exponent yields $\alpha = 1.44 \pm 0.08$). Second, the Bloch's constant from Eq. (4) allows us to calculate the exchange interaction constant A. The best fitting of the experimental data by Eq. (4) corresponds to parameters of M_{s0}=(73.5 ± 0.2) Am^2/kg and $B = (3.13 \pm 0.12) \cdot 10^{-5}$ K$^{-3/2}$.

The obtained B value is similar to the constant for spherical Fe_3O_4 nanoparticles 5 nm in diameter ($B = 3.3 \cdot 10^{-5}$ K$^{-3/2}$) [37]. The exchange interaction constant calculated using the formula $A = \frac{k_B}{8\pi}\left(\frac{M_{s0}}{g\mu_B}\right)^{1/3}\left(\frac{2.612}{B}\right)^{2/3}$ (see, e.g., [38]) was $A = (0.29 \pm 0.02) \cdot 10^{-12}$ J/m. Note that the obtained A value is significantly lower than the exchange constant $A = 7 \cdot 10^{-12}$ J/m of bulk magnetite [39].

The obtained magnetization of particles (73.5 ± 0.2 Am^2/kg) is lower than a value of 92 Am^2/kg for bulk magnetite. A decrease in magnetization can also be associated with non-magnetic additives (unwashed or deposited from the ambient air) on the surface of the particles. The presence of a spin glass shell with the almost zero average magnetization is also discussed as the reason for the decrease in magnetization [4,5]. In ref. [40], the importance of taking into account the two listed contributions to the magnetization is shown and also that the thickness of the spin-glass shell decreases with an increase in the applied field. The experimentally observed reduction in the magnetization of spherical magnetite nanoparticles with an average size of 40 ÷ 45 nm (comparable to the estimate $\sim \sqrt[3]{V} \approx 43$nm for our particles), according to the literature, is $M_s/M_{bulk} = 0.75$ [29]. In our case, $M_s/M_{bulk} = 0.80$, slightly exceeds this value.

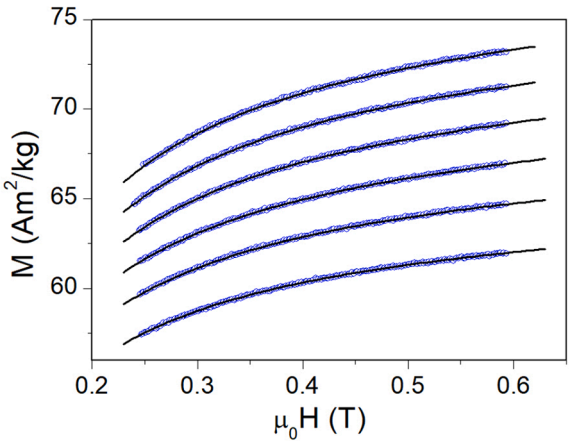

Fig. 5. Approach to magnetic saturation in magnetite nanoplates. Curves were measured at (up to down): 83 K, 125 K, 170 K, 215 K, 253 K, 298 K. The solid lines are the fitting by the Eq. (3).

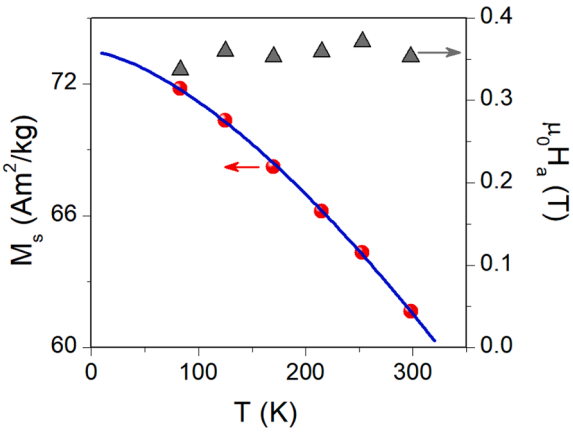

Fig. 6. Saturation magnetization in magnetite particles. The solid line corresponds to Bloch's law (4).

To estimate the magnetic anisotropy constant of a particle, one can use the local magnetic anisotropy field H_a that is best fitting parameter for approach to magnetic saturation fitted by Eq.(3). The values of this field obtained by fitting the curves taken at different temperatures are given in Fig. 6. Since this parameter practically does not change with the particle temperature, it can be characterized by the average value of the anisotropy field. The anisotropy constant recalculated using the local magnetic anisotropy field as $K = H_a M_s/2$ was found to be $K = (6.69 \pm 0.16) \cdot 10^4$ J/m^3.

The magnetic anisotropy constant can also be estimated from the blocking temperature estimate ($T_B = (550 \pm 10)$ K) as $K_{Tb} = 25 \cdot k_B \cdot T_B/V$. Using the average particle volume with the subtracted nonmagnetic shell volume in the calculation, we obtain $K_{Tb} = 3.7 \cdot 10^3 J/m^3$, which is lower by an order of magnitude than the constant estimated from the magnetization curves and theoretical estimates.

The anisotropy constant of the plates exceeds in several times the constant of spherical particles due to the significant contribution of the shape magnetic anisotropy and the larger contribution of the surface. This should lead to the thermal stabilization (blocking) of the magnetic moment for magnetite particles of much smaller volume. In such particles, one may expect a stronger magnetic hysteresis. Indeed, the experimental coercivity H_c(0 K) was found to be 32 mT, whereas the coercivity of spherical magnetite particles is no higher than 10 mT [41]. The upper limit of the H_c value for particles is given by the Stoner–Wohlfarth model, which assumes that particles are single-domain, there is no interaction between them in the ensemble, and magnetization reversal go by coherent rotation. The prediction of this model for the H_c system of randomly oriented particles is $\mu_0 H_c = 0.48 \cdot \frac{2K}{M_s} \approx 170$ mT, where K is the experimentally determined anisotropy constant. This is several times higher than the value $\mu_0 H_c(0\ K) = 32$ mTobtained using Eq. (1) for fitting the data in Fig. 4. One of the reasons for the observed reduction may be the dipole–dipole interaction between particles. Another reason may be the appearance of inhomogeneous states of magnetization within an individual particle. To elucidate this point, we performed the micromagnetic simulation of the hysteresis loops for squared magnetite nanoplate with size similar to the sizes of the particles under study. The modeling of an individual particle is also relevant for biomedical applications. The problem was solved using the OOMMF software [42]. The exchange and magnetization constants and the magnetocrystalline anisotropy in the micromagnetic problem corresponded to the parameters of magnetite. The cubic magnetic anisotropy axes were directed along the plate sides. Modeling shows that the shape of the loop and the value of H_c strongly depend on

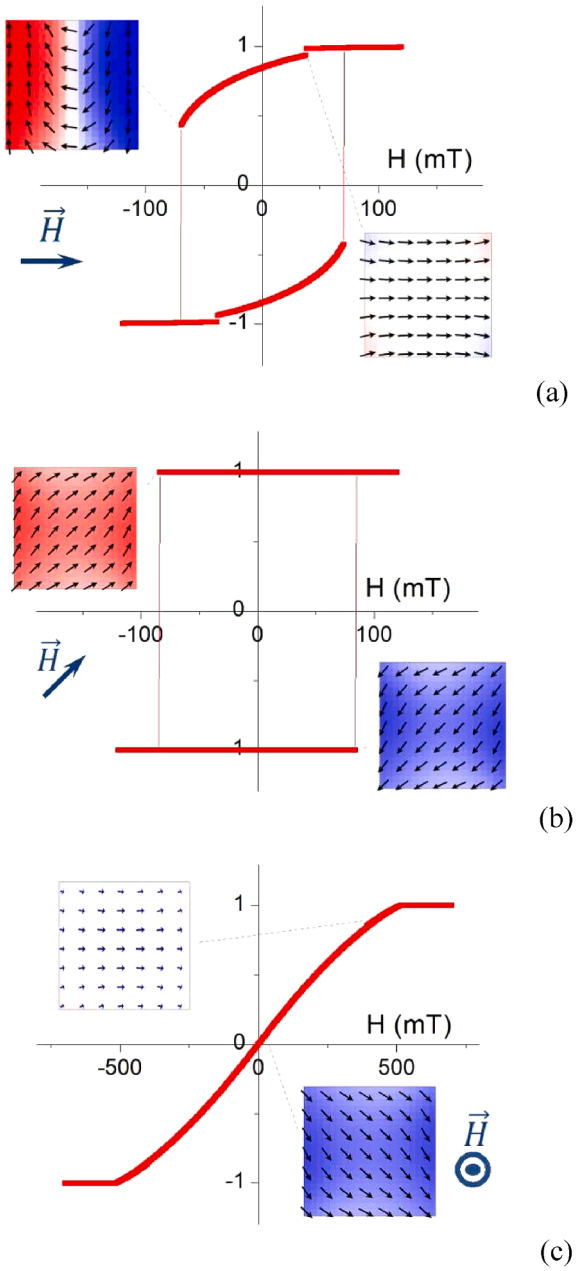

Fig. 7. Calculated hysteresis loops and micromagnetic patterns in magnetite nanoplate (100x100x10nm) at various direction of applied field.

the direction of the field with respect to the plate (Fig. 7). In addition, in the plane of an individual square magnetite plate with dimensions close to the sizes of the obtained particles, inhomogeneous states of magnetization are realized. This means that, upon magnetization reversal, nucleation will occur in fields lower than that predicted by the uniform rotation model. This explains the decrease in observed H_c(0 K) compared to the estimate based on the Stoner–Wohlfarth model.

4. Conclusions

The square plate-shaped magnetite nanocrystals were synthesized by chemical precipitation from solution in the presence of arabinogalactan. The plates had a thickness of 10 ± 3 nm and an average square side of 90 ± 30 nm. In the plate plane, a high crystal quality was observed, while, across the plate, there is some stratification. The particles exhibit the magnetization and temperature stability that are higher than in spherical magnetite particles. The magnetic anisotropy constant larger than that of spherical particles was attributed to the contribution of the shape anisotropy of the plates and the increased contribution of the surface magnetic anisotropy. Nonuniform magnetization patterns revealed by micromagnetic simulation of square ferromagnetic nanoplate and interparticle interactions both should be taken into account for understanding the hysteretic properties of particles at low temperatures. At finite temperatures, hysteresis is significantly reduced by thermal fluctuations.

CRediT authorship contribution statement

S.V. Komogortsev: Data curation, Formal analysis, Writing - original draft, Conceptualization. **S.V. Stolyar:** Supervision, Data curation, Validation, Conceptualization. **L.A. Chekanova:** . **R.N. Yaroslavtsev:** Data curation, Formal analysis, Visualization. **O.A. Bayukov:** . **D.A. Velikanov:** . **M.N. Volochaev:** . **P.E. Eroshenko:** . **R.S. Iskhakov:** Supervision, Writing - review & editing.

Declaration of Competing Interest

The authors declare that they have no known competing financial interests or personal relationships that could have appeared to influence the work reported in this paper.

Acknowledgments

This work was supported by Russian Foundation for Basic Research, Government of Krasnoyarsk Territory, Krasnoyarsk Region Science and Technology Support Fund to the research projects No. 20-42-240001 and 20-42-242902 and by the Council of the President of the Russian Federation for State Support of Young Scientists and Leading Scientific Schools (project no. MK-1263.2020.3). We are grateful to the Center of collective use of FRC KSC SB RAS for the provided equipment.

References

[1] N.A. Usov, A. Zhukov, J. Gonzalez, Single-domain particle with random anisotropy, J. Non Cryst. Solids 353 (2007) 796–798, https://doi.org/10.1016/j.jnoncrysol.2006.12.043.
[2] N.A. Usov, J.M. Barandiarán, Magnetic nanoparticles with combined anisotropy, 053915, J. Appl. Phys. 112 (2012), https://doi.org/10.1063/1.4749799.
[3] V.A. Bautin, A.G. Seferyan, M.S. Nesmeyanov, N.A. Usov, Magnetic properties of polycrystalline cobalt nanoparticles, 045103, AIP Adv. 7 (2017), https://doi.org/10.1063/1.4979889.
[4] R. Kodama, Magnetic nanoparticles, J. Magn. Magn. Mater. 200 (1999) 359–372, https://doi.org/10.1016/S0304-8853(99)00347-9.
[5] R.H. Kodama, A.E. Berkowitz, E.J. McNiff Jr., S. Foner, Surface spin disorder in NiFe2O4 nanoparticles, Phys. Rev. Lett. 77 (1996) 394–397, https://doi.org/10.1103/PhysRevLett.77.394.
[6] G. Cotin, C. Kiefer, F. Perton, D. Ihiawakrim, C. Blanco-Andujar, S. Moldovan, C. Lefevre, O. Ersen, B. Pichon, D. Mertz, S. Bégin-Colin, Unravelling the thermal decomposition parameters for the synthesis of anisotropic iron oxide nanoparticles, Nanomaterials 8 (2018) 881, https://doi.org/10.3390/nano8110881.
[7] G. Marcelo, E. Pérez, T. Corrales, C. Peinado, Stabilization in water of large hydrophobic uniform magnetite cubes by silica coating, J. Phys. Chem. C. 115 (2011) 25247–25256, https://doi.org/10.1021/jp208788k.
[8] D. Kim, N. Lee, M. Park, B.H. Kim, K. An, T. Hyeon, Synthesis of uniform ferrimagnetic magnetite nanocubes, J. Am. Chem. Soc. 131 (2009) 454–455, https://doi.org/10.1021/ja8086906.
[9] T. Wang, X. Wang, D. LaMontagne, Z. Wang, Z. Wang, Y.C. Cao, Shape-controlled synthesis of colloidal superparticles from nanocubes, J. Am. Chem. Soc. 134 (2012) 18225–18228, https://doi.org/10.1021/ja308962w.
[10] G. Singh, H. Chan, T. Udayabhaskararao, E. Gelman, D. Peddis, A. Baskin, G. Leitus, P. Král, R. Klajn, Magnetic field-induced self-assembly of iron oxide nanocubes, Faraday Discuss. 181 (2015) 403–421, https://doi.org/10.1039/C4FD00265B.
[11] A.J. Newell, R.T. Merrill, Nucleation and stability of ferromagnetic states, J. Geophys. Res. Solid Earth. 105 (2000) 19377–19391, https://doi.org/10.1029/2000JB900121.
[12] H.-M. Song, J.I. Zink, N.M. Khashab, Selective magnetic evolution of Mn x Fe 1–x O nanoplates, J. Phys. Chem. C. 119 (2015) 10740–10748, https://doi.org/10.1021/acs.jpcc.5b01938.
[13] A. Rizzuti, M. Dassisti, P. Mastrorilli, M.C. Sportelli, N. Cioffi, R.A. Picca, E. Agostinelli, G. Varvaro, R. Caliandro, Shape-control by microwave-assisted

hydrothermal method for the synthesis of magnetite nanoparticles using organic additives, J. Nanoparticle Res. 17 (2015) 408, https://doi.org/10.1007/s11051-015-3213-0.
[14] S.V. Stolyar, S.V. Komogortsev, L.A. Chekanova, R.N. Yaroslavtsev, O.A. Bayukov, D.A. Velikanov, M.N. Volochaev, E.V. Cheremiskina, M.S. Bairmani, P. E. Eroshenko, R.S. Iskhakov, Magnetite nanocrystals with a high magnetic anisotropy constant due to the particle shape, Tech. Phys. Lett. 45 (2019) 878–881, https://doi.org/10.1134/S1063785019090116.
[15] G. Muscas, G. Concas, C. Cannas, A. Musinu, A. Ardu, F. Orrù, D. Fiorani, S. Laureti, D. Rinaldi, G. Piccaluga, D. Peddis, Magnetic properties of small magnetite nanocrystals, J. Phys. Chem. C. 117 (2013) 23378–23384, https://doi.org/10.1021/jp407863s.
[16] Y. Hadadian, D.R.T. Sampaio, A.P. Ramos, A.A.O. Carneiro, M. Mozaffari, L. C. Cabrelli, T.Z. Pavan, Synthesis and characterization of zinc substituted magnetite nanoparticles and their application to magneto-motive ultrasound imaging, J. Magn. Magn. Mater. 465 (2018) 33–43, https://doi.org/10.1016/j.jmmm.2018.05.069.
[17] J. Yang, Q. Kou, Y. Liu, D. Wang, Z. Lu, L. Chen, Y. Zhang, Y. Wang, Y. Zhang, D. Han, S.G. Xing, Effects of amount of benzyl ether and reaction time on the shape and magnetic properties of Fe3O4 nanocrystals, Powder Technol. 319 (2017) 53–59, https://doi.org/10.1016/j.powtec.2017.06.042.
[18] Z. Nemati, J. Alonso, I. Rodrigo, R. Das, E. Garaio, J.Á. García, I. Orue, M.-H. Phan, H. Srikanth, Improving the heating efficiency of iron oxide nanoparticles by tuning their shape and size, J. Phys. Chem. C. 122 (2018) 2367–2381, https://doi.org/10.1021/acs.jpcc.7b10528.
[19] H. Pfeiffer, Determination of anisotropy field distribution in particle assemblies taking into account thermal fluctuations, Phys. Status Solidi. 118 (1990) 295–306, https://doi.org/10.1002/pssa.2211180133.
[20] R.S. Iskhakov, S.V. Komogortsev, S.V. Stolyar, D.E. Prokof'ev, V.S. Zhigalov, Structure and magnetic properties of nanocrystalline condensates of iron obtained by pulse plasma evaporation, Phys. Met. Metallogr. 88 (1999) 261–269.
[21] S.V. Komogortsev, R.S. Iskhakov, A.D. Balaev, A.V. Okotrub, A.G. Kudashov, N. A. Momot, S.I. Smirnov, Influence of the inhomogeneity of local magnetic parameters on the curves of magnetization in an ensemble of Fe_3C ferromagnetic nanoparticles encapsulated in carbon nanotubes, Phys. Solid State. 51 (2009) 2286–2291, https://doi.org/10.1134/S1063783409110158.
[22] S.V. Komogortsev, R.S. Iskhakov, A.D. Balaev, A.G. Kudashov, A.V. Okotrub, S. I. Smirnov, Magnetic properties of Fe_3C ferromagnetic nanoparticles encapsulated in carbon nanotubes, Phys. Solid State. 49 (2007) 734–738, https://doi.org/10.1134/S1063783407040233.
[23] L. Neel, Théorie du traînage magnétique des ferromagnétiques en grains fins avec application aux terres, Ann. Géophys. 5 (1949) 99–136.
[24] M.P. Sharrock, Time dependence of switching fields in magnetic recording media (invited), J. Appl. Phys. 76 (1994) 6413, https://doi.org/10.1063/1.358282.
[25] N.A. Usov, Y.B. Grebenshchikov, Hysteresis loops of an assembly of superparamagnetic nanoparticles with uniaxial anisotropy, 023917, J. Appl. Phys. 106 (2009), https://doi.org/10.1063/1.3173280.
[26] I.S. Poperechny, Y.L. Raikher, V.I. Stepanov, Dynamic hysteresis of a uniaxial superparamagnet: Semi-adiabatic approximation, Phys. B Condens. Matter. (2013), https://doi.org/10.1016/j.physb.2013.08.049.
[27] J. García-Otero, A. García-Bastida, J. Rivas, Influence of temperature on the coercive field of non-interacting fine magnetic particles, J. Magn. Magn. Mater. 189 (1998) 377–383. doi:10.1016/S0304-8853(98)00243-1.
[28] S.I. Smirnov, S.V. Komogortsev, Magnetization curves of randomly oriented ferromagnetic single-domain nanoparticles with combined symmetry of magnetic anisotropy, J. Magn. Magn. Mater. 320 (2008) 1123–1127, https://doi.org/10.1016/j.jmmm.2007.10.029.
[29] A.P. Safronov, I.V. Beketov, S.V. Komogortsev, G.V. Kurlyandskaya, A.I. Medvedev, D.V. Leiman, A. Larrañaga, S.M. Bhagat, Spherical magnetic nanoparticles fabricated by laser target evaporation, 052135, AIP Adv. 3 (2013), https://doi.org/10.1063/1.4808368.
[30] E.C. Devi, I. Soibam, Law of approach to saturation in Mn–Zn ferrite nanoparticles, J. Supercond. Nov. Magn. (2018), https://doi.org/10.1007/s10948-018-4823-4.
[31] E.C. Devi, I. Soibam, Magnetic properties and law of approach to saturation in Mn-Ni mixed nanoferrites, J. Alloys Compd. 772 (2019) 920–924, https://doi.org/10.1016/j.jallcom.2018.09.160.
[32] S. Mørup, B.R. Hansen, Uniform magnetic excitations in nanoparticles, 024418, Phys. Rev. B. 72 (2005), https://doi.org/10.1103/PhysRevB.72.024418.
[33] S. Mørup, C. Frandsen, M.F. Hansen, Uniform excitations in magnetic nanoparticles, Beilstein J. Nanotechnol. 1 (2010) 48–54, https://doi.org/10.3762/bjnano.1.6.
[34] D. Ortega, E. Vélez-Fort, D.A. García, R. García, R. Litrán, C. Barrera-Solano, M. Ramírez-del-Solar, M. Domínguez, Size and surface effects in the magnetic properties of maghemite and magnetite coated nanoparticles, Philos. Trans. R. Soc. A Math. Phys. Eng. Sci. 368 (2010) 4407–4418, https://doi.org/10.1098/rsta.2010.0172.
[35] P.V. Hendriksen, S. Linderoth, P.-A. Lindgård, Finite-size modifications of the magnetic properties of clusters, Phys. Rev. B. 48 (1993) 7259–7273, https://doi.org/10.1103/PhysRevB.48.7259.
[36] J. Chen, C. Sorensen, K. Klabunde, G. Hadjipanayis, E. Devlin, A. Kostikas, Size-dependent magnetic properties of MnFe2O4 fine particles synthesized by coprecipitation, Phys. Rev. B. 54 (1996) 9288–9296, https://doi.org/10.1103/PhysRevB.54.9288.
[37] G.F. Goya, T.S. Berquó, F.C. Fonseca, M.P. Morales, Static and dynamic magnetic properties of spherical magnetite nanoparticles, J. Appl. Phys. 94 (2003) 3520–3528, https://doi.org/10.1063/1.1599959.
[38] F. Keffer, Handbuch der physik, in: S. Flugge (Ed.), Handb. Der Phys., Springer-Verlag, Berlin, 1966: p. 560.
[39] J.M.D. Coey, Magnetism and magnetic materials, Cambridge University Press, New York, 2010.
[40] D. Zákutná, D. Nižňanský, L.C. Barnsley, E. Babcock, Z. Salhi, A. Feoktystov, D. Honecker, S. Disch, Field dependence of magnetic disorder in nanoparticles, 031019, Phys. Rev. X. 10 (2020), https://doi.org/10.1103/PhysRevX.10.031019.
[41] J. Sung Lee, J. Myung Cha, H. Young Yoon, J.-K. Lee, Y. Keun Kim, Magnetic multi-granule nanoclusters: A model system that exhibits universal size effect of magnetic coercivity, Sci. Rep. 5 (2015) 12135, https://doi.org/10.1038/srep12135.
[42] M.J. Donahue, D.G. Porter, OOMMF user's guide, version 1.0, Gaithersburg, MD, 1999. doi:10.6028/NIST.IR.6376.